Complex Propagators for Evanescent Waves in Bidirectional Beam Propagation Method

Hongling Rao, M. J. Steel, Rob Scarmozzino, *Member, IEEE*, and Richard M. Osgood, Jr., *Fellow, IEEE*

***Abstract*—Existing algorithms for bidirectional optical beam propagation proposed to simulate reflective integrated photonic devices do not propagate evanescent fields correctly. Thus inaccuracy and instability problems can arise when fields have significant evanescent character. We propose complex representations of the propagation operator by choosing either a complex reference wave number or a complex representation of Padé approximation to address this issue. Therefore correct evolution of both propagating waves and evanescent waves can be simultaneously realized, significantly reducing the inaccuracy and instability problems. Both test problems and practical problems are presented for demonstration.**

***Index Terms*—Beam propagation method (BPM), bidirectional, evanescent wave, integrated optics.**

I. Introduction

HE BEAM propagation method (BPM) [1]–[3] has proved to be very useful and popular in numerical simulation of photonic integrated circuit devices because of its accuracy in a large class of practical problems and its efficiency compared to other algorithms [such as finite difference time domain (FDTD)] [4]. As a one-way propagator however, conventional BPM suffers from the well-known deficiency of being unable to treat reflections generated by refractive index variations. To overcome this serious limitation, several bidirectional BPM techniques have been introduced to deal with reflections at a single interface [5]–[7]. These methods are useful for simple problems such as reflection from a single laser facet, or the rear wall of a multimode interference (MMI) device. However, numerous important photonic devices such as gratings or certain add–drop filters contain many reflecting surfaces. Recently we proposed a comprehensive bidirectional formulation [8] to treat systems with an arbitrary number of reflecting interfaces. We demonstrated accurate and efficient modeling of a number of familiar devices such as distributed feedback Bragg gratings, antireflection/high-reflection coatings, and add–drop multiplexers in WDM applications. Previously, a complete description of these devices problems was the domain of resource-intensive FDTD algorithms.[1]

However, a significant weakness remains in current bidirectional BPM techniques—evanescent waves are generated at interfaces but are not propagated correctly by the conventional BPM propagator [10]. This creates two problems. Not only does the incorrect modeling of the evanescent fields add error to the final solution; also these waves can lead to serious instability problems in bidirectional BPM. The examples discussed in [8] did not noticably suffer from these problems because the evanescent portions of the field were not large enough to ruin the stability and the accuracy of the calculations. But there are a number of reflective devices in which the behavior of evanescent waves is critical, as we see in the following section.

In this paper, we counter both of the above problems by using a complex representation for the field propagator, either a complex reference wave number or a complex Padé approximation. The former formulation, suggested by Chang [11], was first mentioned in our previous work [8]. The latter has been used in the context of undersea acoustical wave propagation [12], [13] and was introduced to the integrated optics area by Yevick *et al.* [14]. More precisely, the studies of Yevick *et al.* [14] and ourselves [8] only applied complex operators at interfaces between regions of contrasting refractive index. This procedure correctly generates evanescent field components at the interface itself and in doing so, helps to overcome the most serious stability problems. However, as mentioned above, it does nothing to capture the behavior of the evanescent part of the fields *away* from the interface. The evanescent portion of the fields should of course, grow or decay through a single region. In this paper, we extend the previous studies by applying the complex representation to both interface operators and propagation operators. Thus we are able to both control stability and produce a qualitative as well as quantitative improvement in the representation of the field. Evanescent fields can now decay and grow.

In the next section, we first examine the role of the complex reference wave number/complex Padé approximation and then demonstrate that this idea can enable simultaneous propagation of pure evanescent waves and normal propagating waves. Next, the proposed idea is further demonstrated through comparison with theoretical results on a structure exhibiting frustrated total internal reflection. Finally, as a practical example

Manuscript received November 17, 1999; revised April 27, 2000. This work was supported by DARPA/AFOSR under Contract F49620-99-1-0038, and by a NIST Advanced Technology Program under NIST Cooperative Agreement 70NANB8H4018.

H. Rao, M. J. Steel, and R. M. Osgood, Jr., are with the Microelectronics Sciences Laboratories, Columbia University, New York, NY 10027 USA.

R. Scarmozzino is with RSoft Inc., Ossining, NY 10562 USA.

Publisher Item Identifier S 0733-8724(00)06477-X.

[1]We note that one other BPM investigation [9] has also described a multi-interface algorithm. That formulation however, relied on correctly "guessing" the transmitted field. For most interesting photonic structures however, the output field does not possess a simple form, and, in fact, can have many spatial features including a radiation component, which can not be guessed. In contrast, our formulation is completely general and relies only on a specification of the *input* field as with conventional BPM.

and a challenging problem for bidirectional BPM, a simulation of a T-shaped power splitter is presented.

II. Complex Representation of the Field Propagator

In the bidirectional BPM formulation in [8], the electric field at any point is represented by the two-component vector $U = [u^+(x), u^-(x)]$ of "forward" $(+)$ and "backward" $(-)$ waves. The overall transfer matrix M relating the fields at the front $u^{\pm}_{\text{in}}$ and rear $u^{\pm}_{\text{out}}$ of the structure is defined by

$$\begin{bmatrix} u^+_{\text{out}} \\ u^-_{\text{out}} \end{bmatrix} = M \cdot \begin{bmatrix} u^+_{\text{in}} \\ u^-_{\text{in}} \end{bmatrix}. \tag{1}$$

In some regions, the fields we discuss here are largely evanescent. In that case, the fields u_+ and u_- are more correctly described as "decaying" and "growing" respectively. For convenience we use the forward and backward designations throughout. The matrix M is constructed[2] as

$$M = T_{n,n+1}P_n \ldots P_2 T_{12} P_1 \tag{2}$$

where matrix P_i $(i = 1, 2, \ldots, n)$ stands for the propagation matrix in region i, i.e.

$$P_i = \begin{bmatrix} e^{-i\int \mathcal{L}_i\, dz} & 0 \\ 0 & e^{i\int \mathcal{L}_i\, dz} \end{bmatrix} \tag{3}$$

and $T_{i,i+1}$ for the interface matrix connecting region i and $i+1$, i.e.

$$T_{i,i+1} = \frac{1}{2}\begin{bmatrix} 1+\mathcal{L}_{i+1}^{-1}\mathcal{L}_i & 1-\mathcal{L}_{i+1}^{-1}\mathcal{L}_i \\ 1-\mathcal{L}_{i+1}^{-1}\mathcal{L}_i & 1+\mathcal{L}_{i+1}^{-1}\mathcal{L}_i \end{bmatrix}. \tag{4}$$

Both P_i's and $T_{i,i+1}$'s contain a square-root operator, $\mathcal{L}_i$, which is given by

$$\mathcal{L}_i = \bar{k}\sqrt{1 + \frac{\partial^2/\partial x^2 + n_i(x)^2 k_0^2 - \bar{k}^2}{\bar{k}^2}} \tag{5}$$

where $n_i(x)$ is the index profile in region i, k_0 is the vacuum wave number, $\bar{k}$ is the reference wave number, and where we assume a 2D/TE-polarized case, for simplicity. This square-root operator is usually rationalized by Padé approximants. For instance, in Padé order (n, n)

$$\mathcal{L}_i \approx \bar{k}\left[1 + \sum_{i=1}^{n} \frac{a_i \xi}{1 + b_i \xi}\right] \tag{6}$$

where

$$\xi \equiv \frac{\partial^2/\partial x^2 + n_i(x)^2 k_0^2 - \bar{k}^2}{\bar{k}^2}. \tag{7}$$

If the reference wave number $\bar{k}$ and the Padé coefficients a_i and b_i are all real-valued, then operator $\mathcal{L}_i$ corresponds to a mapping of the real axis onto itself. As a result, although the propagating modes, corresponding to real-to-real mapping, are accurate to the order of the approximation, the evanescent modes, which should be mapped onto the positive imaginary axis, only retain zeroth-order accuracy for any n. Consequently, the evanescent fields generated at the interfaces are treated as propagating fields and cannot decay or grow as they should. Finally, as pointed out in [14], this inappropriate treatment of evanescent modes leads to computational instability, because the evanescent modes are assigned real eigenvalues which can result in a vanishing denominator in evaluation of the reflection operator. Even if the simulation remains stable, calculation of reflection and transmission coefficients can be grossly inaccurate as an evanescent field propagates through the system rather than being localized at an interface [10].

The solution to these inaccuracy and instability problems is to find a better propagator which does not map to the real axis. Two options are to choose a complex-valued reference wave number $\bar{k}$ [8] or to use a complex representation of the Padé approximation [12]–[15]. The former approach is straightforward. A phase factor, φ, is added to the reference wave number

$$\bar{k} = \bar{k}_0 e^{i\varphi} \tag{8}$$

where $\bar{k}_0$ is the original real-valued reference wave number. The latter approach has several alternative schemes [12], [13]. One of them is to rotate the branch cut of the square-root operator in making the Padé approximation [14], [15]. That is, when approximating the operator $\mathcal{L}_i$, the branch cut of the square-root function is rotated away from the original negative real axis

$$\begin{aligned} \mathcal{L}_i = \bar{k}\sqrt{1+\xi} &= \bar{k}e^{i\alpha/2}\sqrt{1+[(1+\xi)e^{-i\alpha}-1]} \\ &\approx \bar{k}e^{i\alpha/2}\left[1 + \sum_{i=1}^{n} \frac{a_i[(1+\xi)e^{-i\alpha}-1]}{1+b_i[(1+\xi)e^{-i\alpha}-1]}\right] \end{aligned} \tag{9}$$

where α is the rotation angle. Note that $\bar{k}$ in the above expression can be either real-valued or complex-valued. We show in the Appendix that the complex $\bar{k}$ method and rotated branch cut method with real-valued $\bar{k}$ are completely equivalent if $\alpha = 2\varphi$. Thus, while we only speak in terms of the complex wave number scheme in the following, all results apply to both pictures.

The literature [8], [14] has so far only used the complex representation on the interface operators to eliminate the interface instability mentioned above. But in some devices, correctly modeling the exponential behavior of the evanescent field propagation can also be critical, from both stability and accuracy points of view. Thus, we have to consider also applying the complex representation when rationalizing $\mathcal{L}_i$ in BPM propagators.

A. Demonstration of the Idea on a Test Problem

In the following test problem, we see that a complex reference wave number can help evanescent fields exponentially decay, without degrading the normal evolution of propagating fields in standard BPM. This is important because in practical devices, the propagating components and evanescent components are usually present at the same time.

In our test problem, a wide Gaussian beam is launched onto an interface between a high permittivity dielectric, say a semiconductor, and air with an incident angle either below or above the critical angle $\sin^{-1}(n_2/n_1)$, as schematically shown in Fig. 1(a) and (b), respectively. Elementary optics states that a normal Gaussian beam propagates beyond the interface in case (a) while

[2]Note that matrix M is never explicitly calculated; only its application to a vector U is required. This is obtained by propagating the "+" and "−" component of the vector forward through the system.

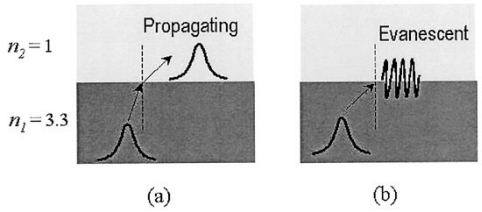

Fig. 1. A Gaussian beam is launched onto an interface between semiconductor and air with an incident angle (a) below the critical angle and (b) above the critical angle. Then propagating Gaussian beam and evanescent field appear on the interface in case (a) and case (b) respectively.

an evanescent wave is generated and localized at the interface in case (b). We use one-way BPM simulation with the complex representation to model the evolution of both fields after the interfaces.

This test problem has exact solutions found by applying the Fresnel formulae to each spatial Fourier component of the incoming beam. The reflected and transmitted beams are obtained by integrating the reflection and transmission of each component over the whole Fourier space. Fig. 2(a) and (b) plots, respectively, the error in power of the propagating beam in case (a) and the error in decay rate of the evanescent field in case (b) as a function of φ. We see that the complex $\bar{k}$ method degrades the normal field propagation but improves the evanescent field propagation. The two figures seem to suggest that some medium value of φ should be used for both fields to propagate accurately. But since they also indicate as expected that the sensitivity to φ falls with increasing Padé order, raising Padé order can always improve the performance in both cases for any nonzero φ.

The results of the above test serve as a necessary condition that the use of the two schemes can be applied to bidirectional BPM.

B. Simulation of Frustrated Total Internal Reflection

We now construct an example in which a complex treatment of the BPM propagator is critical in bidirectional BPM modeling. A structure displaying frustrated total internal reflection (FTIR) is formed by adding another dielectric layer to the top of the structure of case (b) in the previous section with a small air gap. Instead of studying just the propagation of a particular field in a particular region as in the previous section, we are now interested in finding the reflectivity and transmissity of this whole structure with bidirectional BPM. Note that this example is presented here for test purposes, because it again has a convenient analytic solution in the Fourier representation and can also be simulated by rotating the system by 90° and using standard BPM. (Standard BPM solutions could also be used as a reference solution, though here we only compare against the analytic results.)

The refractive index of the dielectric is $n_1 = 3$, the vacuum wavelength is $\lambda = 0.86\ \mu$m, and the angle of incidence $= 30°$. The air gap is chosen to be 0.12 μm thick ($\sim$1 decay length). Using bidirectional BPM without a complex treatment of the propagator (i.e., $\varphi = 0°$), the calculation blows up and we are unable to obtain a solution, even if the instability due to the interface is eliminated by using complex $\bar{k}$ on interfaces.

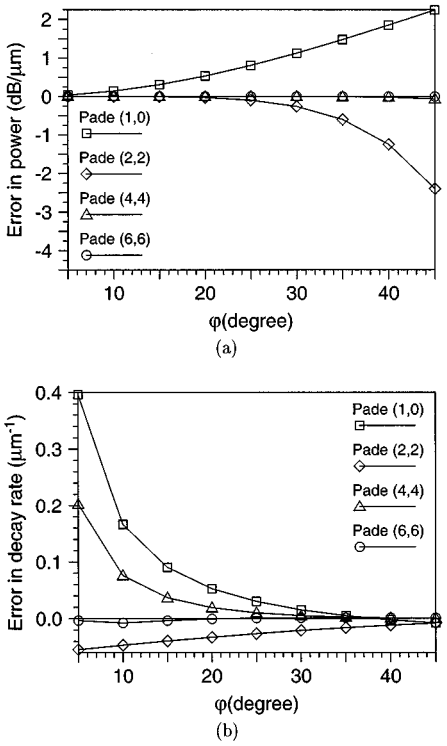

Fig. 2. (a) Error in power of the propagating beam as a function of the angle φ under different Padé orders; (b) Error in decay rate of the evanescent field as a function of φ under different Padé orders.

This behavior occurs as almost 100% of the field present in the air region is evanescent due to the first dielectric/air interface. Physically this field should decay very rapidly, but due to the real-to-real mapping of operator $\mathcal{L}_i$, it propagates as a traveling wave. As an evanescent field, it largely consists of high-frequency spatial components. Thus it essentially acts as a source of noise, and spreading out in all regions, catastrophically degrades the calculation. However, if the complex $\bar{k}$ method (i.e. $\varphi \neq 0°$) is used for the propagation in the air region, then a reasonable solution can be obtained.

Fig. 3(a) shows a field contour pattern obtained by bidirectional BPM when $\varphi = 25°$ in the air layer. A closeup of the field around the air gap is shown in Fig. 3(b). The quantity $\int |E(x)|^2\, dx$, where x is the direction parallel to the interfaces, is measured for the backward field $(E = u_-(x))$, and the total field $(E = u_+(x) + u_-(x))$ over the propagation distance in this closeup region [see Fig. 3(c)]. Comparison with the analytic solution indicates an excellent agreement. Since the scale of the discrepancy is within 1% and would not be visible in the figure, we have excluded the analytic result in Fig. 3(c). In contrast, Fig. 3(d) shows the highly unphysical result obtained when the complex $\bar{k}$ technique is not employed $(\varphi = 0°)$. Notably, for the complex calculation, the backward field in the air gap grows even as the total field energy decays, as theory predicts. This is not seen for $\varphi = 0°$. Thus this simple FTIR problem clearly demonstrates the utility and significance of complex-valued propagation $\bar{k}$.

Fig. 4 plots transmission and total power (reflection + transmission) as a function of φ under different propagation Padé orders. The two dashed lines without symbols mark

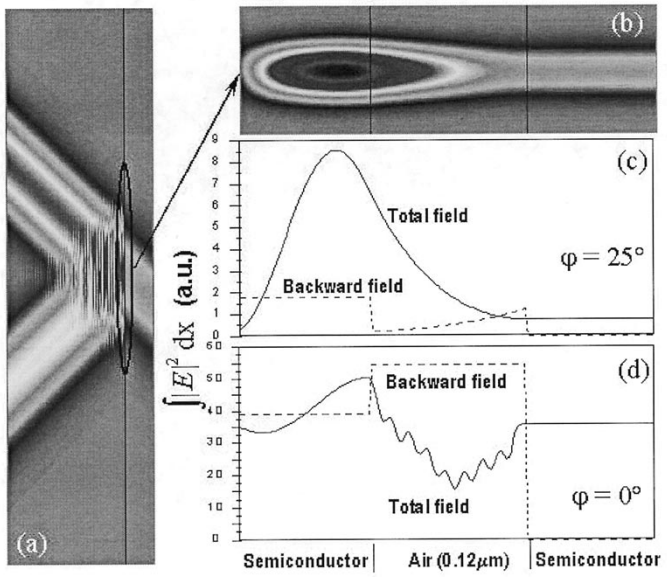

Fig. 3. (a) Field contour pattern of frustrated total internal reflection structure described in the text where the air gap is 0.12 μm thick. It is obtained by bidirectional BPM with complex $\bar{k}$ ($\varphi = 25°$) in air region; (b) The closeup of (a) around the air gap. (The solid lines bound the air gap region); (c) Quantity $\int |E(x)|^2\, dx$ for the total field and the backward field in (b) as a function of propagation distance. They agree with the analytic ones (not shown here) within 1%. For reference, in (d) is also shown this quantity for the total field and the backward field calculated without complex $\bar{k}$ ($\varphi = 0°$) in air region. They are just too unphysical due to the noise problem, as mentioned in the text. (Note: the scales in (a) and (b) are not in proportion with reality.)

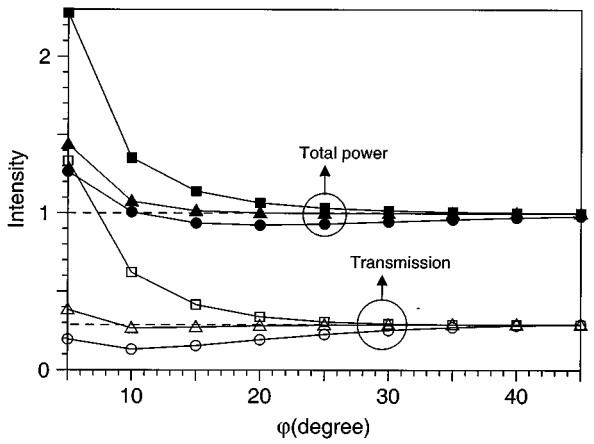

Fig. 4. Transmission and total power (reflection + transmission) as a function of φ under different propagation Padé orders. The two dashed lines without symbols mark the theoretical values of the transmission and total power (unity). The lines with circles, squares and triangles stand for the bidirectional BPM solutions under Padé (3, 3), (5, 5), and (8, 8), respectively.

the theoretical values of the transmission and total power (unity). Again we observe that higher Padé order provides more freedom in choosing the azimuthal angle of $\bar{k}, \varphi$.

Note that the use of the complex reference wave number in the propagator is applied judiciously by restricting it to the air gap region. Analogy with plane-wave optics tells us that little evanescent field is present in regions other than air. If a complex $\bar{k}$ is also used in those regions, normal propagating waves display growing or decaying behavior during simulation which could give rise to instability. We have observed this effect.

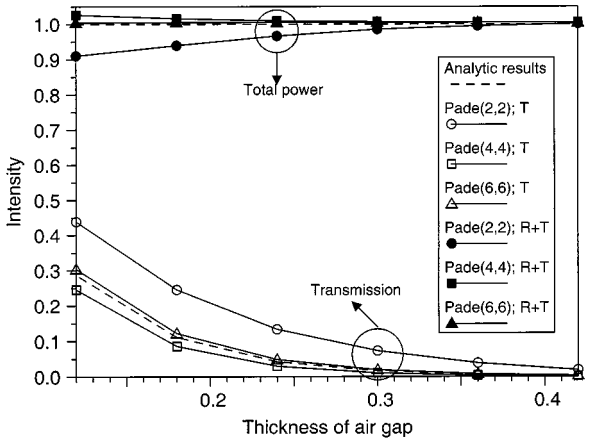

Fig. 5. Dependence of the transmission and total power on the thickness of the air gap under different Padé orders in TE polarization case. The value of φ for the air gap is 25°.

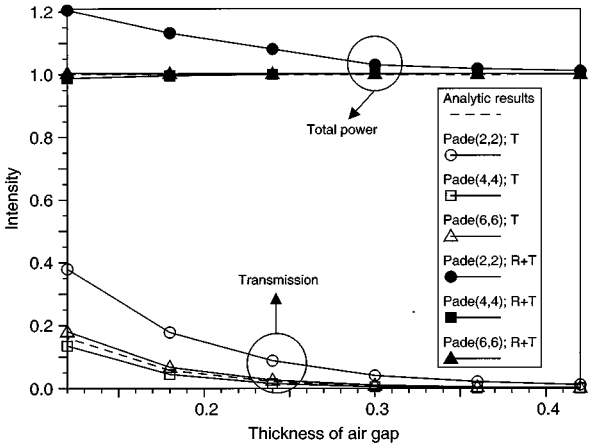

Fig. 6. Dependence of the transmission and total power on the thickness of the air gap under different Padé orders in TM polarization case. The value of φ for the air gap is 25°.

Further calculations are performed to obtain the dependence on thickness of the air gap, as shown in Figs. 5 and 6 for transverse electric (TE) and transverse magnetic (TM) cases, respectively. The value of φ for the air gap is chosen to be 25° and we see that good agreement with analytic results can be achieved with sufficient Padé order.

C. T-Junction Power Splitter

Lastly, we present a more practical structure which requires the current method (if a BPM technique is to be used). It is a T-shaped power splitter taken from Ref. [16][3] as illustrated in Fig. 7(a). A beam coming from the bottom wider waveguide is split into the two narrower waveguides with power equally divided. In the natural orientation [Fig. 7(a)], the whole structure can not be simulated by conventional BPM due to the 90° range in propagation direction, but a bidirectional method works. In the bidirectional approach, the structure is rotated by 45° as shown in Fig. 7(b) and only one interface (the horizontal side of the notch) needs to be considered as a reflecting interface. Thus

[3]A slight change has been made to the original structure by removing the slow tapering in the input waveguide.

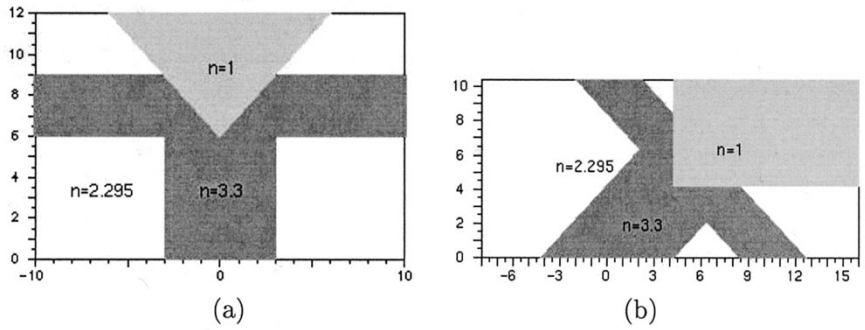

Fig. 7. T-shaped power splitter (a) in normal orientation (b) rotated by 45° to suit the need of bidirectional BPM simulation.

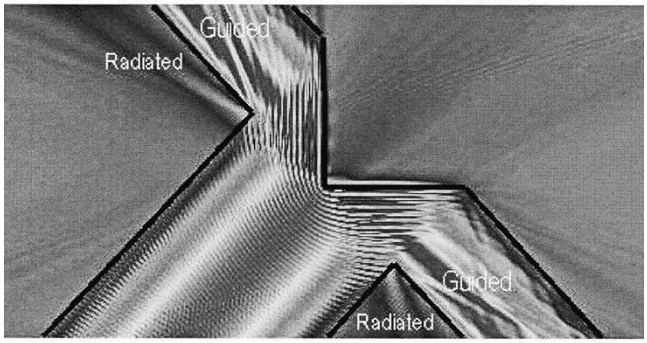

Fig. 8. Simulated field pattern of the T-shaped power splitter obtained by bidirectional BPM with the orientation shown in Fig. 7(b).

the two physically symmetric arms are treated differently in the numerics. The propagation of the reflected field into the top-left arm is taken care of by normal wide-angle BPM, whereas the reflected beam into the bottom-right arm should be handled by the interface reflection operator. Therefore, this problem is a challenging test for bidirectional BPM as well as a practical example. Note that beyond the horizontal interface, both the propagating component on the left and the evanescent component on the right have to be propagated correctly at the same time. Thus we require the use of a complex representation of the propagator.

Fig. 8 shows a contour plot of the beam splitting simulated by bidirectional BPM with φ chosen as 12° in a finite region ($\sim$0.7 wavelength) after the interface. The symmetry is basically preserved but not perfectly, e.g., the two radiation beams scattered from the corners at the junction travel into the cladding region $(n = 2.295)$ at different angles, and the powers in each outgoing arm are 39 and 41%, respectively. This is of course a penalty for treating the structure in an asymmetric manner as we are forced to do in order to apply a BPM technique. Our discussion of Fig. 2 suggests the result could in principle be improved by raising the Padé order in propagation since only Padé order (1, 1) was used to obtain Fig. 8. However, we have found that for this example, applying a high order Padé algorithm prevents us from obtaining stable solutions. This notwithstanding, our method permits a BPM approach of reasonable accuracy to a problem that is otherwise completely inaccessible to BPM techniques.

III. Conclusion

We have proposed and demonstrated the use of complex treatment of the propagation operator to properly handle the propagation of evanescent waves in bidirectional BPM simulations. Our method mitigates the inaccuracy and instabilities which are otherwise encountered. The complex treatment of the propagation operator can be made either through a complex reference wave number or a complex representation of Padé approximation (say, rotated branch cut Padé approximation).

Appendix
Equivalence of Complex Reference Wave Number Method and Rotated Branch Cut Padé Approximation Method

Below we refer to the complex reference wave number method as method A and rotated branch cut Padé approximation as method B.

In method A, combining (6)–(8), the approximation of operator $\mathcal{L}_i$ is rewritten as

$$\mathcal{L}_i \approx \mathcal{L}_i^{(A)} \equiv \bar{k}_0 e^{i\varphi}\left[1+\sum_{i=1}^{n}\frac{a_i\xi}{1+b_i\xi}\right]. \tag{10}$$

In method B, when $\bar{k}$ in rotated branch cut Padé approximation is real-valued, i.e., $\bar{k}=\bar{k}_0, \xi$ becomes

$$\xi_0 \equiv \frac{\partial^2/\partial x^2 + n_i(x)^2 k_0^2 - \bar{k}_0^2}{\bar{k}_0^2}. \tag{11}$$

According to (9), operator $\mathcal{L}_i$ in method B is approximated as

$$\begin{aligned}\mathcal{L}_i &\approx \mathcal{L}_i^{(B)} \\ &\equiv \bar{k}_0 e^{i\alpha/2}\left[1+\sum_{i=1}^{n}\frac{a_i[(1+\xi_0)e^{-i\alpha}-1]}{1+b_i[(1+\xi_0)e^{-i\alpha}-1]}\right].\end{aligned} \tag{12}$$

Comparing (11) to (7), we obtain

$$(1+\xi_0)e^{-2i\varphi} = 1+\xi \tag{13}$$

Thus, (12) is rewritten as

$$\mathcal{L}_i^{(B)} = \bar{k}_0 e^{i\alpha/2}\left[1+\sum_{i=1}^{n}\frac{a_i\xi}{1+b_i\xi}\right]. \tag{14}$$

By applying (8) again and comparing (10) and (14), it is readily seen that $\mathcal{L}_i^{(B)} = \mathcal{L}_i^{(A)}$.

REFERENCES

[1] D. Yevick and B. Hermansson, "Efficient beam propagation techniques," *IEEE J. Quantum Electron.*, vol. 26, pp. 109–112, 1990.

[2] Y. Chung and N. Dagli, "An assessment of finite difference beam propagation methods," *IEEE J. Quantum Electron.*, vol. 26, pp. 1335–1339, 1990.

[3] R. Scarmozzino and R. M. Osgood Jr., "Comparison of finite-difference and Fourier-transform solutions of the parabolic wave equation with emphasis on integrated-optics problems," *J. Opt. Soc. Amer. A*, vol. 8, pp. 724–729, 1991.

[4] W. P. Huang, S. T. Chu, A. Goss, and S. K. Chaudhuri, "A scalar finite-difference time-domain approach to guided-wave optics," *IEEE Photon. Technol. Lett.*, vol. 3, pp. 524–526, 1991.

[5] P. Kaczmarski and P. E. Lagasse, "Bidirectional beam propagation method," *Electron. Lett.*, vol. 24, pp. 675–676, 1988.

[6] Y. Chiou and H. Chang, "Analysis of optical waveguide discontinuities using the padé approximants," *IEEE Photon. Technol. Lett.*, vol. 9, pp. 964–966, 1997.

[7] C. Yu and D. Yevick, "Application of the bidirectional parabolic equation method to optical waveguide facets," *J. Opt. Soc. Amer. A*, vol. 14, pp. 1448–1450, 1997.

[8] H. Rao, R. Scarmozzino, and R. M. Osgood Jr., "A bidirectional beam propagation method for multiple dielectric interfaces," *IEEE Photon. Technol. Lett.*, vol. 7, pp. 830–832, 1999.

[9] Y. Chung and N. Dagli, "Modeling of guided-wave optical components with efficient finite-difference beam propagation methods," *Proc. IEEE Antennas Propagat. Soc. Int. Symp., 1992 Dig.*, vol. 1, pp. 248–251, 1992.

[10] H. E. Hernández-Figueroa, "Simple Nonparaxial Beam-Propagation Scheme for Integrated Optics," *J. Lightwave Technol.*, vol. 12, pp. 644–649, 1994.

[11] H.-C. Chang, "Department of Electrical Engineering and Graduate Institute of Electro-Optical Engineering, National Taiwan University, Taipei 106–17, Taiwan, China, 1997, Private communication," unpublished.

[12] M. D. Collins, "Higher-order padé approximations for accurate and stable elastic parabolic equations with application to interface wave propagation," *J. Acoust. Soc. Amer.*, vol. 89, pp. 1050–1057, 1991.

[13] ——, "A two-way parabolic equation for elastic media," *J. Acoust. Soc. Amer.*, vol. 93, pp. 1815–1825, 1993.

[14] H. El-Refaei, D. Yevick, and I. Betty, "Padé approximation analysis of reflection at optical waveguide facets," *Proc. 1999 Tech. Dig., Integr. Photon. Res.*, pp. 104–106, 1999.

[15] F. A. Milinazzo, C. A. Zala, and G. H. Brooke, "Rational square-root approximations for parabolic equation algorithms," *J. Acoust. Soc. Amer.*, vol. 101, pp. 760–766, 1997.

[16] W. Yang and A. Gopinath, "A boundary integral method for propagation problems in integrated optical structures," *IEEE Photon. Technol. Lett.*, vol. 7, pp. 777–779, 1995.

Hongling Rao, photograph and biography not available at the time of publication.

M. J. Steel, photograph and biography not available at the time of publication.

Rob Scarmozzino (M'98), photograph and biography not available at the time of publication.

Richard M. Osgood, Jr. (SM'82–F'87), photograph and biography not available at the time of publication.